Clean Technologies and Environmental Policy (2018) 20:2201–2208
https://doi.org/10.1007/s10098-018-1528-0

ORIGINAL PAPER

Effect of Mn substitution on the oxidation/adsorption abilities of iron(III) oxyhydroxides

Dong-Wan Cho[1] · Chul-Min Chon[2] · Hyuncheol Yang[1,2] · Yiu Fai Tsang[3] · Hocheol Song[1]

Received: 7 January 2018 / Accepted: 10 April 2018 / Published online: 19 April 2018

Abstract

In this study, divalent manganese ions [Mn(II)] were substituted a part of divalent iron ions [Fe(II)] present in Fe oxyhydroxides to prepare novel composites (Mn@Feox). The composites were prepared by (1) simultaneous hydrolysis of Fe(II) and Mn(II), and (2) rapid oxidation with H_2O_2. The resulting Mn@Feox prepared with different molar ratios of Fe and Mn was characterized and evaluated for their abilities to adsorb arsenic species [As(III) and As(V)] in aqueous solution. X-ray diffraction and field emission transmission electron microscope analyses revealed Mn@Feox has a δ-(Fe_{1-x}, Mn_x)OOH-like structure with their mineralogical properties resembling those of feroxyhyte (δ-FeOOH). The increase in Mn substitution in Mn@Feox enhanced the oxidative ability to oxidize As(III) to As(V), but it decreased the adsorption capacity for both arsenic species. The optimal Mn/Fe molar ratio that could endow oxidation and magnetic capabilities to the composite without significantly compromising As adsorption capability was determined to be 0.1 (0.1Mn@Feox). The adsorption of As(III) on 0.1Mn@Feox was weakly influenced by pH change while As(V) adsorption showed high dependence on pH, achieving nearly complete removal at pH < 5.7 but gradual decrease at pH > 5.7. The adsorption kinetics and isotherms of As(III) and As(V) showed good conformity to pseudo-second-order kinetics model and Freundlich model, respectively.

Keywords Iron oxide · Manganese · Magnetic composite · Arsenic · Oxidation · Adsorption

Introduction

Iron(III) oxides or oxyhydroxides are some of the most common minerals found in the environment with varying contents of iron, oxygen, hydroxyl and other anions (CO_3^{2-}, SO_4^{2-} and Cl^-), and occur naturally as four types of iron polymorphs (α, β, γ and δ). Among those iron polymorphs, FeOOH groups are of a special interest due to their large surface area and high adsorption capability toward dissolved contaminants (Li et al. 2017; Rosso and Rustad 2001). In particular, removal of anionic contaminants such as As(V), fluoride and phosphate can be efficiently removed by iron oxyhydroxides via an exchange reaction (Kumar et al. 2009). For this reason, many researchers have investigated the adsorption of anionic contaminants by Fe(III) oxyhydroxides (Jang et al. 2009; Kyzas and Matis 2015; Majzlan 2011; Muller et al. 2010). For example, Müller et al. (2010) found feroxyhyte (δ-FeOOH) readily binds to arsenic species by formation of arsenic–iron oxide complex. Majzlan (2011) found that hydrous ferri oxide (HFO, akaganéite, β-FeOOH) has a good affinity to As(V), and HFO-loaded granular activated carbon (GAC) showed better adsorption capacity of As(V) (26 mg As g^{-1}) than pristine GAC (Jang et al. 2009).

Recently, attempts to fabricate bi-functional composites that possess both oxidation and adsorption capabilities have been made (Mei et al. 2015; Tang et al. 2016; Zhang et al. 2014; Qi et al. 2015). One prominent example of such materials is binary oxides composed of manganese (Mn)- and iron (Fe) oxides. Mn oxides in the composite serve as a mild oxidant for redox active pollutants, while Fe oxides

Electronic supplementary material The online version of this article (https://doi.org/10.1007/s10098-018-1528-0) contains supplementary material, which is available to authorized users.

✉ Hocheol Song
hcsong@sejong.ac.kr

[1] Department of Environment and Energy, Sejong University, Seoul 143-747, Korea

[2] Geologic Environment Division, Korea Institute of Geoscience and Mineral Resources, Daejeon 305-350, Korea

[3] Department of Science and Environmental Studies, The Education University of Hong Kong, Tai Po, New Territories, Hong Kong

provide adsorbing surface as well as magnetic property to the composite (Fang et al. 2017). Mn/Fe oxides showed good performance in degradation of tetracycline under microwave irradiation (Gu et al. 2017). The nanocomposites consisting of Fe_3O_4/MnO_2 successfully degraded methylene blue dye (Mei et al. 2015). Mn/Fe oxides also showed enhanced treatment capability for heavy metals [Cd(II), Cu(II), Pb(II), Zn(II) and As(III)] as compared to single-phase Fe oxides (Kim et al. 2013; Zhao et al. 2016; Zhang et al. 2007).

Arsenic species mainly exist in the forms of As(III) (H_3AsO_3, $H_2AsO_3^-$ and $HAsO_3^{2-}$) and As(V) ($H_2AsO_4^-$, $HAsO_4^{2-}$ and AsO_4^{3-}) in aqueous phase. In general, As(III) is more toxic and is less effectively removed by Fe-based adsorbents as compared to As(V) under the general condition except highly alkaline condition (Li et al. 2012). Thus, pre-oxidation of As(III) to As(V) could be a feasible option for better treatment of As. Xiong et al. (2017) fabricated MnO_2/FeOOH/carbon composites and achieved high adsorption of As(III) (75.8 mg g^{-1}) at pH 3. However, the adsorption of As(III) and As(V) on Mn/Fe oxides is highly dependent upon pH condition due to charge variation of arsenic species and Mn/Fe oxides. When Mn is incorporated into Fe oxides phases, it tends to decrease point of zero charge due to strong negative charges of Mn oxides (Chon et al. 2018). Given that the typical pH range for surface/groundwater is 6.5–8.5, the surface of Mn/Fe oxides exhibit net negative charge, therefore adsorption of negatively charged As(V) ions produced by peroxidation of As(III) may not be favored.

Consequently, it is desirable to find the optimal content of Mn in the binary composite despite the demonstrated advantages of Mn incorporation in treating arsenic. The objective of this study was to fabricate a Mn/Fe binary oxide (Mn@Feox) with oxidation capability for use as a treatment medium for arsenic species, As(III) and As(V). The physicochemical characteristics of Mn@Feox prepared at different molar ratio of Mn/Fe were examined using various instrumentation. The adsorption capability of composites for As(III) and As(V) was evaluated with final pH effect, adsorption kinetic and adsorption isotherm experiments.

Experimental

Materials

Anhydrous sodium arsenite salt ($NaAsO_2$), sodium arsenate salt (Na_2HAsO_4), sodium nitrate salts ($NaNO_3$), manganese chloride salt ($MnCl_2$), ferrous chloride salt ($FeCl_2$), chromium (III) chloride ($CrCl_3$), 30% hydrogen peroxide (H_2O_2) and 1 N NaOH solution were purchased from Sigma-Aldrich, USA. Sodium nitrate ($NaNO_3$) was obtained form OCI co., Korea. The reagents were used without further purification. Stock solutions (1000 mg L^{-1}) of As(III) and As(V) were prepared, respectively, by dissolving corresponding amounts of salts of sodium arsenite and sodium arsenate in distilled water. Ferrous chloride solution of 12.6 g L^{-1} (0.1 M) was also prepared in a similar manner.

Preparation of Mn/Fe composites

Mn-incorporated iron oxyhydroxides (Mnox@Feox) were prepared by modifying the method developed by Schwertmann and Cornell (2000). $FeCl_2$ solutions containing varying molar ratios of Mn (0, 10, 30 and 50%) relative to Fe were prepared by adding the corresponding amounts of $MnCl_2$ into the 12.6 g L^{-1} $FeCl_2$ solutions, and pH of the suspensions was elevated to 12 by dropwise addition of 1 N NaOH. The solutions started to form black precipitates with the increase in pH and were further mixed with 200 mL of 30% H_2O_2 for 10 min at constant stirring to rapidly oxidize Mn(II) and Fe(II) to Mn(IV) and Fe(III) on the precipitated minerals, respectively. Upon the oxidation, the color of precipitates turned blackish brown and the pH decreased to neutral. The resulting materials were washed several times with distilled deionized water, freeze-dried for 24 h and kept in sealed bottles until use. The adsorbents having the different Mn/Fe molar ratios (0, 0.1, 0.3 and 0.5) were named as Feox, 0.1Mnox@Feox, 0.3Mnox@Feox and 0.5Mnox@Feox, respectively.

Adsorption experiments

Adsorption experiments to investigate the effect of Fe and Mn contents in Mnox@Feox on As(III) and As(V) adsorption were carried out in 25 mL vials. The experiments were conducted in duplicate, and the average values of raw data were used as experimental results. The vials received 0.02 g Mn@Feox, followed by addition of 20 mL of either 59.4 mg L^{-1} As(III) or 58.2 mg L^{-1} As(V) solution. The pH was adjusted to 6 by adding 0.1 N HCl or NaOH, and the ionic strength was set at 10 mM by dissolving $NaNO_3$ salts. The vials were mixed at 150 rpm and 25 ± 2 °C in a water bath shaker. At given time intervals, samples were collected and filtered with 0.45 μm syringe filter (Pall Co., USA), followed by measurement of the concentrations of arsenic species in the solutions. The effect of pH on the arsenic adsorption was investigated by adding 0.02 g adsorbent into the vials containing 20 mg L^{-1} As(III) or As(V) solutions in the final pH range of 2–9. For adsorption kinetic experiments with different concentrations of As(III) and As(V), 0.02 g Mn@Feox was added to each of 20 mL of arsenic solutions [As(III): 19.5, 52.7 and 96.7 mg L^{-1}, As(V): 19.4, 48.1 and 98.0 mg L^{-1}]. Adsorption isotherm experiments were carried out with solutions of As(III) and As(V) concentrations in the ranges of 47.7–228.4 and 30.3–241.1 mg L^{-1}, respectively, using 1 g L^{-1} Mn@Feox. The total concentrations of arsenic [As(III) + As(V)] in aqueous solution were determined by an

inductively coupled plasma (ICP-OES, Ultima 2C, Horiba, Japan). A SAX cartridge (Alltech, USA), an anion exchange resin, was used to remove As(V) from the solution (Amirbahman et al. 2006). As(III) concentration in the eluent was measured with the ICP, and the As(V) concentration was calculated by subtracting As(III) concentration from the total As concentration. The pH of solution was measured by a pH meter (Horiba, Japan).

Characterization of Mn@Feox

The particle size distribution and the morphology of Mn@Feox samples were measured using a field emission transmission electron microscope (FE-TEM, JEM-2200FS, JEOL). X-ray diffractometer (D8 Advance, Bruker-AXS) analyses were performed to characterize the mineralogical phases of Mn@Feox using Cu Kα radiation and a LynxEye position sensitive detector. The diffraction pattern was collected from 10° to 95° 2θ, with a nominal step size of 0.01° and a time per step of 1 s, using a 0.3° divergence slit and 2.5° secondary Soller slit.

The Rietveld structural refinement (Rietveld 1969) was performed with TOPAS 4.2 (Bruker, Germany) program to evaluate the crystal structural changes with the incorporation of Mn. Standard chromium net oxidation test (SCNOT) proposed by Bartlett and James (1979) was conducted to measure the oxidative capacity of Mn@Feox samples as follows: The vial containing 2.5 g of Mn@Feox and 25 mL of 1 mM $CrCl_3$ was shaken for 2 h. Then, 0.25 mL of 1 M phosphate buffer solution (pH 7.2) was added to remove sorbed Cr(VI), and the vial was shaken for 15 s. Supernatant was collected after centrifugation and filtrated with a 0.45 μm syringe filter. The concentration of chromate [Cr(VI)] in the supernatant was measured by s-diphenyl carbazide direct colorimetric method (USEPA 1995). The measured concentration of produced Cr(VI) corresponds to oxidative capacity of Mn@Feox. The zeta potential values were measured using a Zetasizer Nano ZS instrument (Malvern, UK) in the range of equilibrium pH values of 2.78–8.72, to determine the pH at the point of zero charge (pH_{pzc}) of Mn@Feox. Magnetic susceptibility of Mn@Feox was measured using a Bartington MS2 magnetic susceptibility meter (UK).

Results and discussion

Characterization of Mn@Feox

FE-TEM images of Mn@Feox showed hexagonal thin-plate morphology with a [001] preferential orientation, and the size of each plate particles ranged in 20–60 nm (Fig. 1). No obvious structural changes were observed when Mn ratio of the precursor solution was increased (Fig. 1b–d), which

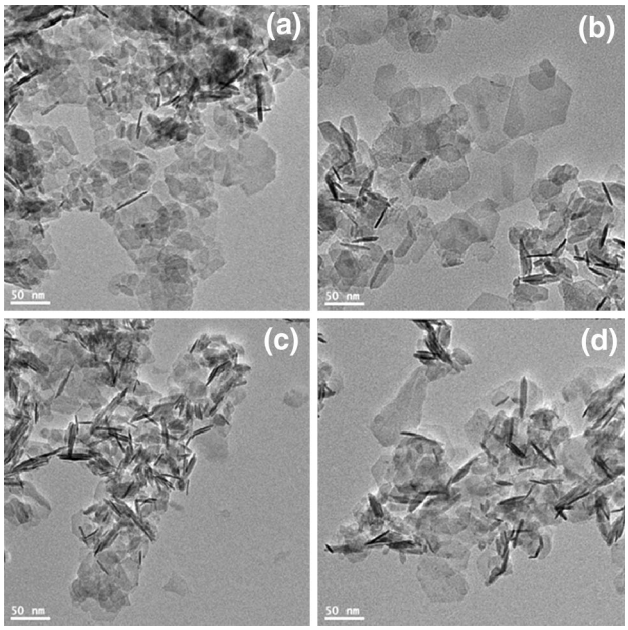

Fig. 1 FE-TEM images of **a** Feox, **b** 0.1Mn@Feox, **c** 0.3Mn@Feox and **d** 0.5Mn@Feox

implies that the incorporation of Mn did not lead to formation of identifiable Mn oxide phases.

The XRD of Feox showed peaks at 35.8°, 40.2°, 54.2° and 62.8° (Fig. 2a), which correspond to (100), (101), (102) and (110) planes of δ-FeOOH, respectively (JCPDS No. 13-0087) (Chukhrov et al. 1977). These peaks were also observed for 0.5Mn@Feox, with no other peaks attributable to Mn oxide phases being found (Fig. 2b). This observation suggests that the addition of Mn did not form separate Mn oxide phases, but it was substituted into Fe oxides framework, which is consistent with the result of FE-TEM. One interesting observation in the XRD spectra was the significant change in the unit cell parameters of Mn@Feox (Fig. 2c). Rietveld refinement analysis of XRD data revealed that the unit cell volume (v) and a-axis lattice (a) proportionally decreased with increasing Mn content, which has a good agreement with the changes in the crystal structure parameters by Mn substitution as reported previously (Sileo et al. 2001). This means that Mn effectively substituted Fe in δ-FeOOH in proportion to the added Mn without formation of other single phases of Mn.

The results of SCNOT test to evaluate the effect of Mn content on the oxidative capacity of Mn@Feox are presented in Table 1. The oxidation capabilities of Mn@Feox significantly increased with increasing Mn content, giving the highest Cr(III) oxidation capability of 18.44 mmol Cr(VI) kg^{-1} for 0.5Mn@Feox. On the other hand, the magnetic susceptibility of Mn@Feox was substantially reduced by about 200 times (3.65E−05 $m^3\ kg^{-1} \rightarrow$ 1.71E−07 $m^3\ kg^{-1}$) when the Mn/Fe ratio increased to 0.5, which can lead to the failure of magnetic separation after the use. Given the opposite relationship between

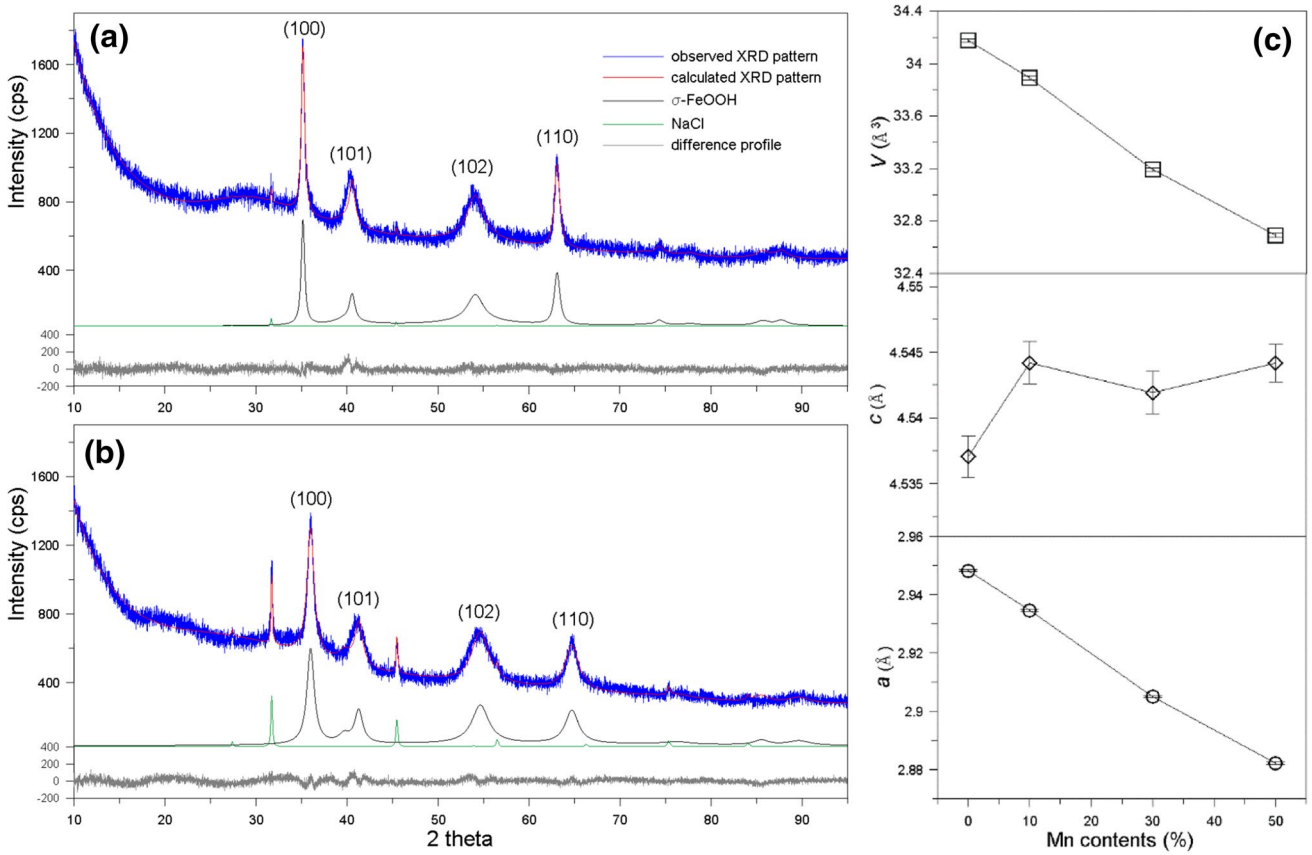

Fig. 2 XRD patterns of **a** Feox and **b** 0.5Mn@Feox; and **c** Rietveld refinement results and crystal structural changes of different Mn@Feoxs. *v: cell volume, a: a-axis lattice, c: c-axis lattice

Table 1 Oxidative capacities and magnetic susceptibilities of Mn@Feox composites

Sample	Generated Cr(VI) conc. (mmol kg^{-1})	Magnetic susceptibility (m^3 kg^{-1})
Feoxs	0.018	3.65E−05
0.1Mn@Feoxs	2.804	9.00E−06
0.3Mn@Feoxs	7.786	1.27E−06
0.5Mn@Feoxs	18.44	1.71E−07

two properties, the excessive use of Mn in the fabrication of Mn@Feox is not desirable from a practical standpoint.

Figure 3 presents the results of zeta potential measurements of Mn@Feox. Feox showed positive potential values at pH < 8, and charge reversal to a negative value occurred at around 8. The increase in Mn content resulted in a shift of pH_{pzc} to lower values down to 6.2 for 0.5Mn@Feox. This is likely due to the contribution from Mn that possesses high concentration of surface hydroxyl groups (Tamura et al. 1989). For this reason, Mn oxides typically exhibit the relatively lower pH_{pzc} values (0.96–3.3) compared to Fe oxides (Hou et al. 2016; Lopano et al. 2007).

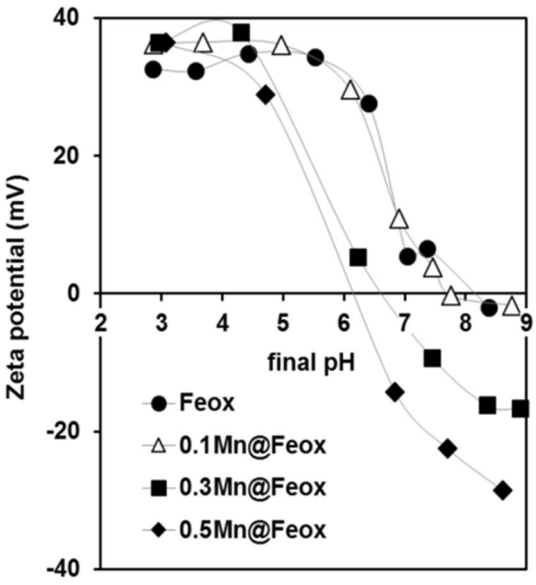

Fig. 3 Zeta potential values (mV) of different Mn@Feoxs (Feox, 0.1Mn@Feox, 0.3Mn@Feox, and 0.5Mn@Feox) with varying pH values (final pH range 2.7–9.0)

Effect of Mn substitution on arsenic adsorption

Figure 4a shows the adsorption capacities of Feox and Mn@Feox for As(III) and As(V). The increase in Mn content decreased the adsorption of As, resulting in 33.5 and 53.4% decrease of As(III) and As(V) when Fe/Mn molar ratio increased from 0 to 0.5, respectively (Fig. 4a). This decrease in As adsorption is likely related to reduced availability of iron oxide phases in Mn@Feox with increasing Mn content. The lower values of pHpzc of Mn@Feox as compared to unsubstituted Feox also contributed to the decrease in As adsorption since the surface would develop negative charges. In As(III) adsorption by Mn@Feox, it is assumed that As(III) is either directly adsorbed or oxidized into As(V) followed by adsorption onto the surface. After completion of adsorption experiments, As(III) was not detected in all the reacted As(III) solutions, but the concentration of residual As(V) increased with the increasing Mn content in Mn@Feox (Fig. 4b). This observation indicates that the increase in Mn led to more oxidation ability of composite due to the increase in number of reactive species (i.e., reduced Mn ions).

A similar route of As(III) to As(V) oxidation and subsequent As(V) adsorption has been documented in previous work that utilized iron minerals containing MnOOH or Mn species (Gupta et al. 2010; Lakshmipathiraj et al. 2006). This work was aimed to fabricate Mn-substituted Fe composites without significantly compromising adsorption capability of Fe oxide phase. Therefore, 0.1Mn@Feox with good magnetic property was chosen among the Mn@Feoxs for further experiments.

Effect of final pH on As adsorption

The results of As(III) and As(V) adsorption by 0.1Mn@Feox at varying pH conditions are presented in Fig. 5. The reactions were allowed to occur for 24 h with a Mn@Feox dose of 1 g L^{-1}, and As(III) and As(V) concentrations of 19.4 and 19.5 mg L^{-1}. Note that the pH values reported in the figure are the final pH values at the end of reactions. The results indicated As(III) adsorption showed a weak parabolic behavior with the pH change, showing maximum adsorption at mid pH range (5.5–7.2). However, there was only a small difference between the maximum and minimum values of As(III) adsorption (88–96%) over the entire pH range. This suggests As(III) adsorption was weakly influenced by the pH-dependent surface charge of Mn@Feox. A similar pattern of As(III) adsorption on iron oxides under varying pH condition has been reported by other researchers (Dixit and Hering 2003; Jang et al. 2006).

On the contrary, As(V) adsorption showed an apparent dependence on pH such that nearly complete removal was obtained in low pH conditions (pH < 5.7), while it declined continuously from pH 5.7 to 9.0. The high adsorption of As(V) under low pH conditions could be attributed to electrostatic

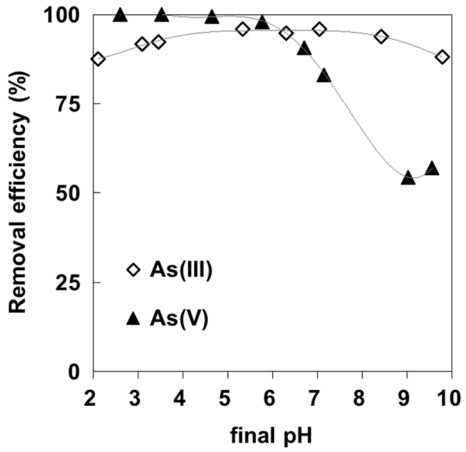

Fig. 5 Effect of final pH on the adsorption of As(III) and As(V) by 0.1Mn@Feox [Adsorbent dose = 1 g L^{-1}; initial As(III) and As(V) concentrations = 19.4 and 19.5 mg L^{-1}]

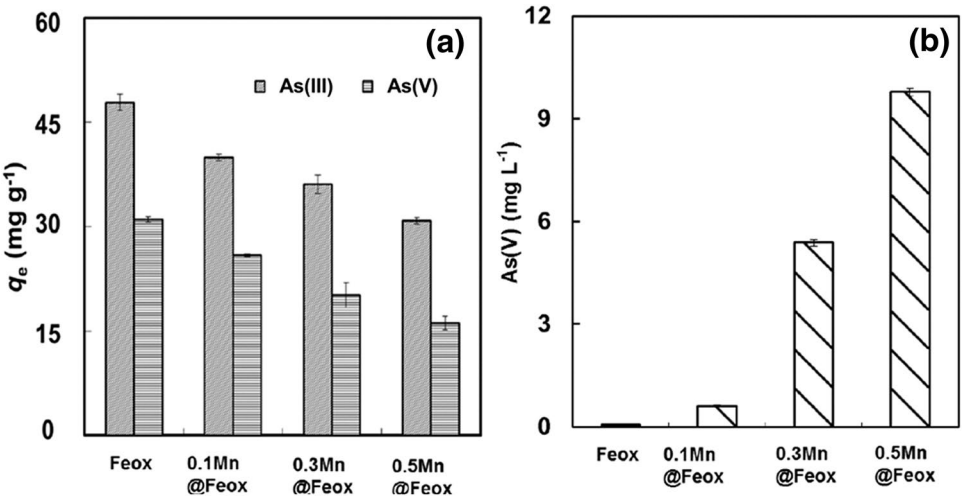

Fig. 4 **a** Adsorbed amount (mg g^{-1}) of As(III) and As(V) by different Mn@Feoxs (Feox, 0.1Mn@Feox, 0.3Mn@Feox and 0.5Mn@Feox) and **b** As(V) concentration in the reacted As(III) solutions of Mn@Feoxs [Adsorbent dose = 1 g L^{-1}, initial pH 6, final pH 8.0–8.2 initial As(III) and As(V) concentrations = 59.4 and 58.2 mg L^{-1}, contact time = 24 h]

interaction between positively charged surface and negatively charged As(V). As shown in Fig. 3, zeta potential values of 0.1Mn@Feox were in the positive range at pH < 6, and this led to attraction of As(V) that mainly present as negatively charged ion ($H_2AsO_4^-$) at corresponding pH range. In a similar context, further increase in pH significantly reduced positive charge density on Mn@Feox and resulted in limited access of As(V) to the adsorption sites. Dixit and Hering (2003) obtained a similar pH dependence of As(V) adsorption by ferrihydrite [$Fe(OH)_3$].

Adsorption kinetics and isotherms

Figure 6 presents the adsorption kinetics of arsenic species on 0.1Mn@Feox with initial As(III) (19.5, 52.7 and 96.7 mg L^{-1}) and As(V) (19.4, 48.1 and 98.0 mg L^{-1}) concentrations during 1440 min reactions, respectively. Typically, over 70% of the total adsorption occurred in the first 70 min reaction, and subsequently, saturation of adsorption was reached in 600 min.

To elucidate the adsorption mechanism, pseudo-first-order kinetics and pseudo-second-order kinetic models were used to fit the experimental data. The used kinetics model equations and relevant information were provided in Supplementary Information. The related kinetics parameters for As(III) and As(V) adsorption are summarized in Table 2. The best fits over the entire time range were found with the pseudo-second-order model, indicating the importance of chemical adsorption of As(III) and As(V) onto the active sites of 0.1Mn@Feox.

The maximum adsorbed amounts of As(III) and As(V) by 0.1Mn@Feox as determined by adsorption isotherm experiments were 58.3 and 28.4 mg g^{-1} at initial concentration of 228.4 As(III) and 241.1 As(V) mg L^{-1}, respectively (Fig. 7). The maximum adsorption capacities obtained from the Langmuir model were 57.8 and 27.93 mg g^{-1} for As(III) and As(V), respectively (Table 3). The correlation coefficients of

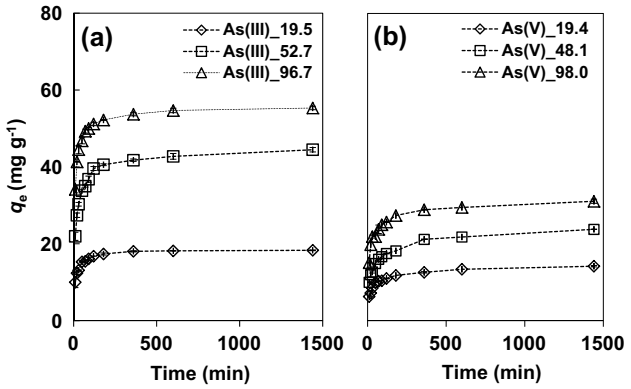

Fig. 6 Adsorption kinetics of **a** As(III) and **b** As(V) by 0.1Mn@Feox at different initial concentrations [Adsorbent dose = 1 g L^{-1}; initial pH 6; final pH 8, Initial As(III) and As(V) concentrations = 19.5, 52.7 and 96.7 mg L^{-1} and 19.4, 48.1 and 98.0 mg L^{-1}]

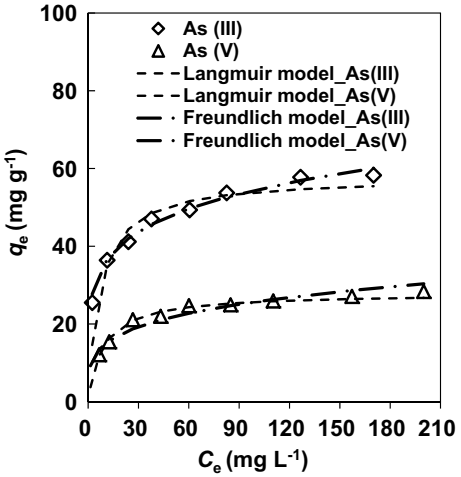

Fig. 7 Adsorption isotherm of As(III) and As(V) by 0.1Mn@Feox [Adsorbent dose = 1 g L^{-1}; initial pH 6; final pH 8; initial As(III) and As(V) concentration ranges = 47.7–228.4 and 30.3–241.1 mg L^{-1}]

Table 2 Kinetics parameters for the adsorption of As(III) and As(V) at three initial concentrations [calculated value = q_e (cal), experimental value = q_e (exp)]

		Pseudo-first order kinetics model			Pseudo-second-order kinetics model		
Initial concentrations (mg L^{-1})	q_e (exp) (mg g^{-1})	k_1 (L min^{-1})	q_e (cal) (mg g^{-1})	R^2	k_2 (g (mg $min)^{-1}$)	q_e (cal) (mg g^{-1})	R^2
As(III)							
19.5	18.3	0.0069	5.0	0.9223	0.0047	18.5	0.9999
52.7	42.9	0.0078	14.1	0.9577	0.0017	43.7	0.9998
96.7	54.8	0.0081	12.8	0.9622	0.0022	55.2	0.9999
As(V)							
19.4	14.2	0.0037	5.8	0.9197	0.0033	13.2	0.9986
48.1	23.8	0.0032	10.8	0.9157	0.0017	22.6	0.9978
98.0	31.1	0.0035	10.2	0.8650	0.0021	30.1	0.9996

Table 3 Adsorption isotherm parameters for 0.1Mn@Feox adsorbent

	q_m (mg g^{-1})	b (L mg)	R^2	k_f (mg g^{-1}) (mg $L^{-1})^{-n}$	n	R^2
As(III)	57.80	0.138	0.9858	23.50	5.47	0.9840
As(V)	27.93	0.112	0.9511	8.56	4.19	0.9363

Langmuir model for As(III) and As(V) adsorption (0.9858 and 0.9511) were higher than those of the Freundlich model (0.9840 and 0.9363). The observed n values of 5.47 and 4.19 indicate that sorption is favorable over the entire range of concentrations examined.

Conclusions

Manganese-substituted Fe oxyhydroxides were prepared using co-precipitation procedure by varying the molar ratio of Fe and Mn (Mn ratio: 0, 10, 30, 50%) in the precursor solutions. XRD analysis of Mn@Feox indicated the main hexagonal framework is feroxyhyte (δ-FeOOH) with Mn substitution in the lattice. The Mn substitution decreased pH_{pzc} of Mn@Feox, and it negatively influenced adsorption of As(V). Although Mn substitution decreased the magnetic susceptibility, 0.1Mn@Feox exhibited sufficient magnetism to be separable by magnetic separation. Mn@Feox showed good oxidation capability to oxidize As(III) to As(V). The adsorption kinetics of As(III) and As(V) by 0.1Mn@Feox was better described by pseudo-second-order kinetics model, and the adsorption isotherm showed a good conformity to the Freundlich model. As a result, the incorporation of Mn at appropriate ratio can impart oxidation ability without a substantial loss of adsorption ability of Fe oxides while maintaining good magnetic property.

Acknowledgements This work was supported, in part, by the Energy Efficiency and Resources of the Korea Institute of Energy Technology Evaluation and Planning (KETEP) granted financial resource from the Ministry of Trade, Industry and Energy, Republic of Korea (No. 20152510101880), and, in part, by the Basic Research Project (15-3414) of the Korea Institute of Geoscience and Mineral Resources (KIGAM), funded by the Ministry of Science, ICT.

References

Amirbahman A, Kent DB, Curtis GP, Davis JA (2006) Kinetics of sorption and abiotic oxidation of arsenic(III) by aquifer materials. Geochim Cosmochim Acta 70:533–547

Bartlett R, James B (1979) Behavior of chromium in soils. 3 Oxidation. J Environ Qual 8:31–35

Chon CM, Cho DW, Nam IH, Kim JG, Song H (2018) Fabrication of Fe/Mn oxide composite adsorbents for adsorptive removal of zinc and phosphate. J Soils Sediments 18:946–956

Chukhrov EV, Zvyagin BB, Gorshkov AJ, Yermilova LP, Korovushkin VV, Rudnitszkaya YS, Yakubovskaya NY (1977) Feroxyhyte, a new modification of FeOOH. Int Geol Rev 19:873–890

Dixit S, Hering JG (2003) Comparison of arsenic(V) and arsenic(III) sorption onto iron oxide minerals: Implications for arsenic mobility. Environ Sci Technol 37:4182–4189

Fang NJ, Guo JX, Shu S, Luo HD, Chu YH, Li JJ (2017) Enhancement of low-temperature activity and sulfur resistance of $Fe_{0.3}Mn_{0.5}Zr_{0.2}$ catalyst for NO removal by NH_3-SCR. Chem Eng J 325:114–123

Gu WL, Lv GC, Liao LB, Yang CX, Liu H, Nebendahl I, Li ZH (2017) Fabrication of Fe-doped birnessite with tunable electron spin magnetic moments for the degradation of tetracycline under microwave irradiation. J Hazard Mater 338:428–436

Gupta K, Maity A, Ghosh UC (2010) Manganese associated nanoparticles agglomerate of iron(III) oxide: synthesis, characterization and arsenic(III) sorption behavior with mechanism. J Hazard Mater 184:832–842

Hou JT, Luo JL, Hu ZQ, Li YZ, Mao MY, Song SX, Liao QL, Li QZ (2016) Tremendous effect of oxygen vacancy defects on the oxidation of arsenite to arsenate on cryptomelane-type manganese oxide. Chem Eng J 306:597–606

Jang M, Min SH, Kim TH, Park JK (2006) Removal of arsenite and arsenate using hydrous ferric oxide incorporated into naturally occurring porous diatomite. Environ Sci Technol 40:1636–1643

Jang M, Cannon FS, Parette RB, Yoon SJ, Chen WF (2009) Combined hydrous ferric oxide and quaternary ammonium surfactant tailoring of granular activated carbon for concurrent arsenate and perchlorate removal. Water Res 43:3133–3143

Kim EJ, Lee CS, Chang YY, Chang YS (2013) Hierarchically structured manganese oxide-coated magnetic nanocomposites for the efficient removal of heavy metal ions from aqueous systems. ACS Appl Mater Interfaces 5:9628–9634

Kumar E, Bhatnagar A, Ji M, Jung W, Lee SH, Kim SJ, Lee G, Song H, Choi JY, Yang JS, Jeon BH (2009) Defluoridation from aqueous solutions by granular ferric hydroxide (GFH). Water Res 43:490–498

Kyzas GZ, Matis KA (2015) Nanoadsorbents for pollutants removal: a review. J Mol Liq 203:159–168

Lakshmipathiraj P, Narasimhan BRV, Prabhakar S, Raju GB (2006) Adsorption studies of arsenic on Mn-substituted iron oxyhydroxide. J Colloid Interface Sci 304:317–322

Li X, He K, Pan BC, Zhang SJ, Lu L, Zhang WM (2012) Efficient As(III) removal by macroporous anion exchanger-supported Fe–Mn binary oxide: behavior and mechanism. Chem Eng J 193:131–138

Li P, Ma X, Li H, Li S, Wu H, Xu D, Zheng G, Fan Q (2017) Sorption mechanism of Th(IV)at iron oxyhydroxide (IOHO)/water interface: batch, model and spectroscopic studies. J Mol Liq 241:478–485

Lopano CL, Heaney P, Post JE, Hanson J, Komarneni S (2007) Time-resolved structural analysis of K- and Ba-exchange reactions with synthetic Na-birnessite using synchrotron X-ray diffraction. Am Mineral 92:380–387

Majzlan J (2011) Thermodynamic Stabilization of Hydrous Ferric Oxide by Adsorption of Phosphate and Arsenate. Environ Sci Technol 45:4726–4732

Mei J, Zhang L, Niu Y (2015) Fabrication of the magnetic manganese dioxide/graphene nanocomposite and its application in dye removal from the aqueous solution at room temperature. Mater Res Bull 70:82–86

Muller K, Ciminelli VST, Dantas MSS, Willscher S (2010) A comparative study of As(III) and As(V) in aqueous solutions and adsorbed on iron oxy-hydroxides by Raman spectroscopy. Water Res 44:5660–5672

Qi J, Zhang G, Li H (2015) Efficient removal of arsenic from water using a granular adsorbent: Fe–Mn binary oxide impregnated chitosan bead. Bioresour Technol 193:243–249

Rietveld HM (1969) A profile refinement method for nuclear and magnetic structures. J Appl Cryst 2:65–71

Rosso KM, Rustad JR (2001) Structures and energies of AlOOH and FeOOH polymorphs from plane wave pseudopotential calculations. Am Miner 86:312–317

Schwertmann U, Cornell RM (2000) Iron oxide in the laboratory: preparation and characterization. Willey, New York

Sileo EE, Alvarez M, Rueda EH (2001) Structural studies on the manganese for iron substitution in the synthetic goethite—jacobsite system. Int J Inorg Mater 3:271–279

Tamura H, Oda T, Furuichi R (1989) Acid-base dissociation of surface hydroxyl groups on manganese dioxide in aqueous solutions. J Electrochem Soc 136:2782–2786

Tang SF, Yuan DL, Zhang Q, Liu YM, Zhang Q, Liu ZQ, Huang HM (2016) Fe-Mn bi-metallic oxides loaded on granular activated carbon to enhance dye removal by catalytic ozonation. Environ Sci Pollut Res 23:18800–18808

USEPA (1995) Standard method 7196A: chromium, hexavalent (colorimetric). Test methods for evaluating solid waste, physical/chemical methods. SW-846, 3rd edn. U.S. Environmental Protection Agency, Washington

Xiong Y, Tong Q, Shan WJ, Xing ZQ, Wang YJ, Wen SQ, Lou ZN (2017) Arsenic transformation and adsorption by iron hydroxide/manganese dioxide doped straw activated carbon. Appl Surf Sci 416:618–627

Zhang G, Qu J, Liu H, Liu R, Wu R (2007) Preparation and evaluation of a novel Fe–Mn binary oxide adsorbent for effective arsenite removal. Water Res 41:1921–1928

Zhang G, Liu F, Liu H, Qu J, Liu R (2014) Respective role of Fe and Mn oxide contents for arsenic sorption in iron and manganese binary oxide: an X-ray absorption spectroscopy investigation. Environ Sci Technol 48:10316–10322

Zhao JH, Liu J, Li N, Wang W, Nan J, Zhao ZW, Cui FY (2016) Highly efficient removal of bivalent heavy metals from aqueous systems by magnetic porous Fe_3O_4–MnO_2: adsorption behavior and process study. Chem Eng J 304:737–746